1 Propagation diagrams for B16 models

The essence of the B16 envelope models is that the enthalpy flux is not just given by a term proportional to the super-adiabatic gradient, but there is an additional term, $-\tau\langle s^2\rangle \boldsymbol{g}\rho T/c_p$, also called the Deardorff term, which carries enthalpy outward, even in layers that are (weakly) Schwarzschild-stable.

The deeper layers of the convection zone can indeed be weakly Schwarzschild-stable when the Deardorff term is driven by mechanical stirring through descending plumes. This phenomenon is superficially reminiscent of overshoot, but, unlike standard overshoot where the enthalpy flux is inward, the Deardorff flux is always outward.

Given the presence of Schwarzschild-stable layers, there is the possibility of trapping g-modes closer to the surface. The question is therefore what their properties are and whether they could be observable. In the following, we compute wave propagation diagrams for such models. When comparing with earlier propagation diagrams that employed standard mixing length models, it should be noted that the B16 envelope models employed simplistic prescriptions for the opacity and ignored partial ionization effects. They also ignored the spherical geometry, i.e., gravity and total flux were constant, instead of varying like r^{-2}. (In reality, $4\pi r^2 F_{\rm tot}$ and $4\pi r^2 g_{\rm r}$ would be constant.) The depth of the convection zone was in all cases less than 200 Mm, so the bottom of the convection zone was at a fractional radius r/R that was larger than 0.7. Furthermore, the propagation diagrams will be unrealistic in the deeper parts due to the neglect of spherical effects, but they may still give an idea about the anticipated effects.

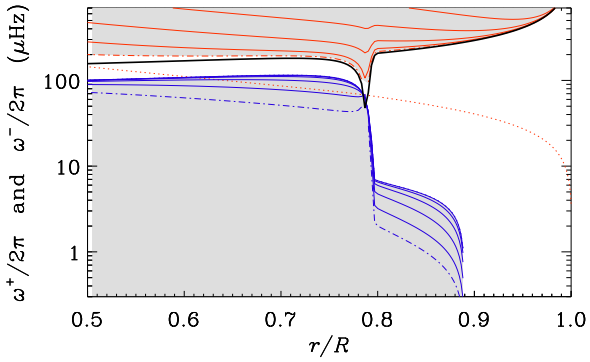

Figure 1: Case I, beta=tbeta=0, fs0=0.3, Fig.4, green line, `pmodels_nabD1_xi1p5_kfHp00`

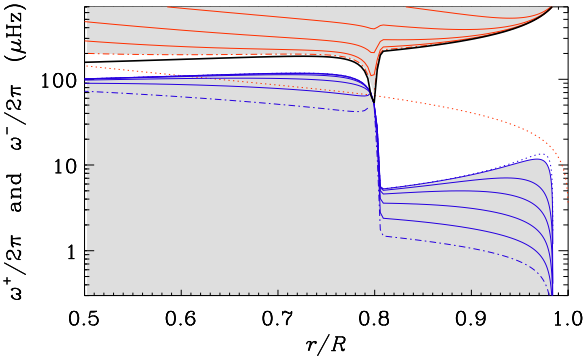

Figure 2: Case II, beta=0, tbeta=1, fs0=0.1, Fig.5, blue line, `pmodels_nabD2_xi1p5_kfHp01`

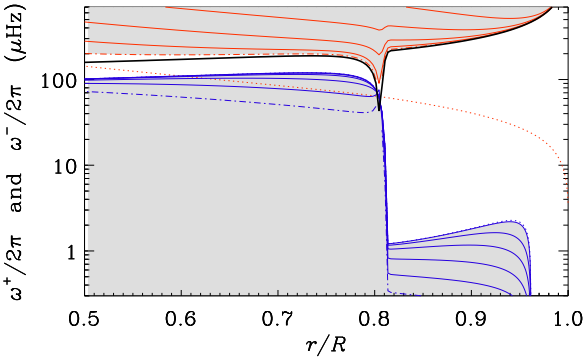

Figure 3: Case III, beta=tbeta=1, fs0=0.1, Fig.6, blue line, `pmodels_nabD2_xi1p5_kfHp`

Figures 1–3 show propagation diagrams similar to those in Appourchaux+10. The frequencies $\omega^\pm$ are the zeros of the function

$$K(r) = \frac{1}{c_{\rm s}^2}\left[\omega^2 - \omega_{\rm c}^2 - S_\ell^2\left(1-\frac{N^2}{\omega^2}\right)\right], \quad (1)$$

where ω is the eigenfrequency, $\omega_{\rm c} = (c_{\rm s}/2H_{\rm p})\sqrt{1-2{\rm d}H_{\rm p}/{\rm d}r}$ is the acoustic cutoff frequency, $S_\ell = \sqrt{\ell(\ell+1)}c_{\rm s}/r$ is the Lamb frequency, and $N = \sqrt{g({\rm d}(s/c_p)/{\rm d}r}$ is the Brunt-Väisälä frequency. The term $K(r)$ enters in the equation

$$\frac{\partial^2\Psi}{\partial r^2} + K(r)\Psi = 0, \quad (2)$$

where Ψ is the eigenfunction, which is proportional to the divergence of the displacement $\boldsymbol{\xi}$ of the relevant mode.

We see that both ω^+ and ω^- increase with ℓ, but ω^+ increases faster, so that the gap between them increases with increasing ℓ.